RAA 2016 Vol. **16** No. **8**, 123(8pp) doi: 10.1088/1674–4527/16/8/123
http://www.raa-journal.org *http://iopscience.iop.org/raa*

Research in Astronomy and Astrophysics

Conceptual Design of the Aluminum Reflector Antenna for DATE5

Yuan Qian[1,2], Frank W. Kan[3], Andrew T. Sarawit[3], Zheng Lou[1,2], Jing-Quan Cheng[1,2], Hai-Ren Wang[1,2], Ying-Xi Zuo[1,2] and Ji Yang[1,2]

[1] Purple Mountain Observatory, Chinese Academy of Sciences, Nanjing 210008, China; *yuanqian@pmo.ac.cn*
[2] Key Laboratory for Radio Astronomy, Chinese Academy of Sciences, Nanjing 210008, China
[3] Simpson Gumpertz and Heger Inc., Waltham, MA 02453, USA

Received 2015 December 21; accepted 2016 April 8

Abstract DATE5, a 5 m telescope for terahertz exploration, was proposed for acquiring observations at Dome A, Antarctica. In order to observe the terahertz spectrum, it is necessary to maintain high surface accuracy in the the antenna when it is exposed to Antarctic weather conditions. Structural analysis shows that both machined aluminum and carbon fiber reinforced plastic (CFRP) panels can meet surface accuracy requirements. In this paper, one design concept based on aluminum panels is introduced. This includes panel layout, details on panel support, design of a CFRP backup structure, and detailed finite element analysis. Modal, gravity and thermal analysis are all performed and surface deformations of the main reflector are evaluated for all load cases. At the end of the paper, the manufacture of a prototype panel is also described. Based on these results, we found that using smaller aluminum reflector panels has the potential to meet the surface requirements in the harsh Dome A environment.

Key words: methods: analytical — methods: numerical — telescopes — techniques: radar astronomy

1 INTRODUCTION

The 5 m Dome A Terahertz Explorer (DATE5) was proposed to explore the unique terahertz observing window available at Dome A (Yang et al. 2013). Table 1 lists the major design specifications of the DATE5 antenna.

In the conceptual design study phase for DATE5, a candidate antenna design for DATE5 was proposed based on machined aluminum panels and a carbon fiber reinforced polymer (CFRP) backup structure (BUS). Aluminum panels have the advantages of being lightweight, low cost, thermally stable, and easily fabricated (Ali et al. 2011; Maldague et al. 1995; Yan & Chen 2012). They have also been used on various submillimeter telescopes in recent years (Fig. 1) (Leong et al. 2006; Kooi et al. 2004; Raffin et al. 2000; Ezawa et al. 2004; Ruhl et al. 2004; Ukita et al. 2004; Lapeyre et al. 2008).

Aluminum panels have performed very well in a number of submillimeter wavelength telescopes as shown in Figure 1. However, their large coefficient of thermal expansion (CTE) can negatively affect the surface accuracy when the antenna is exposed to the large seasonal and vertical temperature variations at Dome A (Xiao et al. 2008). It remains unclear whether aluminum panels are capable of satisfying the surface error budget for DATE5 under conditions at Dome A. In order to address these issues, more structural design and analysis for reducing thermally induced surface error are necessary.

In Section 2, the conceptual design of aluminum reflector panels for DATE5 is introduced in detail. It focuses on the arrangement of panels, the panel support structure and the BUS. In Section 3, a finite element model of the antenna is provided and structural simulations are performed to obtain surface and pointing root mean square (rms) errors of the antenna. Section 4 provides a conclusion and summary of the aluminum reflector panel design for DATE5.

Table 1 Design Specifications of the DATE5 Antenna

Item	Specification
Operating wavelength	350 μm
	200 μm
Primary reflector	5 m aperture diameter
Total surface error	10 μm rms
Absolute pointing error	2″ rms

2 STRUCTURAL DETAILS OF ALUMINUM PANEL DESIGN

For the design of an antenna that uses aluminum panels, the main reflector will still be segmented for reducing thermally induced deformation and overcoming difficulties in the manufacture process. As shown in Figure 2, each panel is thin walled with rib stiffeners on the back so that it is lightweight, but high in stiffness and strength. There are

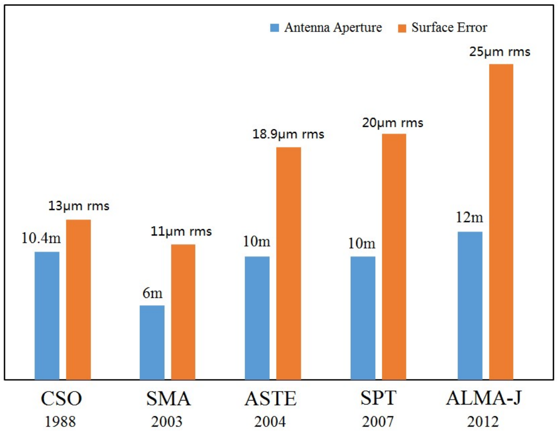

Fig. 1 Major parameters associated with various submillimeter telescopes.

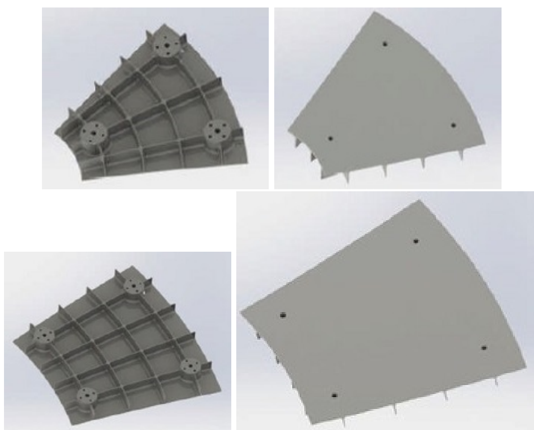

Fig. 2 Front and back views of the aluminum panels.

many sources of error in the surface of the main reflector. However, the most serious one is the thermal deformation caused by the size of the panel. For studying the effect of size on the surface error, two layouts for panels that can be used in the main reflector were studied in the conceptual design phase. One utilizes a smaller panel size and the other is larger as shown in Figure 3. The layout for the larger panels only has three rings of panel segments. The total number of panels is 32 and the number of adjusters is 144. The size of the largest panel is about 0.8 m× 1.1m. The layout for the smaller panels has six rings of panel segments. The total number of panels is 120 and the number of adjusters is 472. The size of the largest panel in this group is only about 0.4 m×0.6 m. For both designs, the gap between panels is 1 mm. The large panel layout has much fewer panels and supports, which makes it easier and faster for on-site alignment at Dome A. However, the thermally induced distortions from seasonal temperature variation can cause significantly larger surface errors than for the smaller panels, as discussed in the next section.

In the BUS design, the main reflector consists of eight segments (see Fig. 4) for both larger and smaller panels. Each segment is sized so that it fits in a 20 ft standard shipping container. The main reflector together with the panels it supports can be shipped together inside the container. Each BUS segment takes the form of a box consisting of two types of stiffeners, radial ones and circumferential ones, and two plate structures, top and bottom ones. The top plate includes openings for the panel support system which is connected to the circumferential stiffeners near the bottom plate. CFRP is selected as the material for the BUS structure instead of aluminum, because the thermal deformation of an aluminum BUS will cause a significant temperature gradient and surface errors. Such surface errors result in unacceptable surface and pointing accuracies.

Since the aluminum panels have a much larger CTE than the CFRP BUS, the surface error of the main reflector will be reduced only if the panels are allowed to expand unconstrained when temperature changes. All the panels are supported by a number of adjusters (Fig. 5). In each adjuster, there are two flexures: one is on top and the other is on bottom. The adjuster flexure planes are arranged so that the normals of the flexure planes are pointing to the center of the panel. This allows a free expansion of the panel on the top of the BUS, which has much lower expansion. The adjuster used is motorized. The motorized adjuster can perform fast on-site surface adjustment of the main reflector at Dome A. This becomes even more important when a large number of adjusters are required. Inside the adjusters, compression springs are used to insure that they are both backlash free and there is no rotation/movement action when making fine height adjustments.

3 NUMERICAL SIMULATIONS

To investigate the feasibility of the above mentioned design, two finite element models are developed: one is for the larger panel layout and the other for the smaller panel layout. Both models, which rely on finite element analysis (FEA), are used for predicting surface and pointing errors of the main reflector under various loading conditions at Dome A. These include thermal, wind and gravity loading. Among these, deformations of the reflector from gravity and thermal loadings are the most important.

Figure 6 shows the finite element model for the DATE5 antenna. In the model, the main reflector panels are modeled with thin shell elements. The subreflector, its positioning system and the counterweight are modeled as lump masses. The BUS and apex are also modeled with shell elements. The panel supports, quadrapod, crown transition structure, mount and truss pedestal are modeled with beam elements. The parameters of the models for larger and smaller panel layouts are listed in Table 2.

The mass of the smaller panel model is slightly heavier than that of the larger panel model as more adjusters are used in the smaller panel model. In order to house these more adjusters, the BUS structure for the smaller panel model is more rigid.

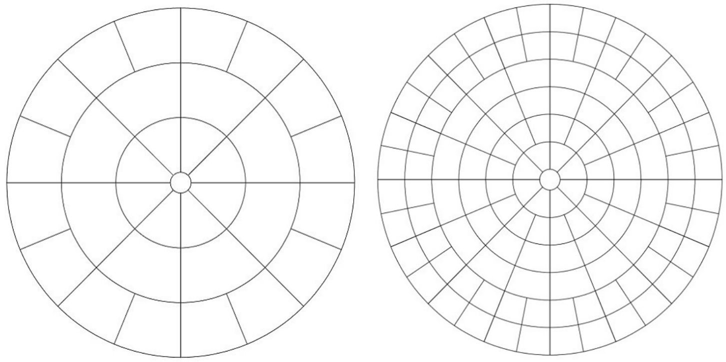

Fig. 3 Layout schemes of the main reflector: the large panel layout (*left*) and small panel layout (*right*).

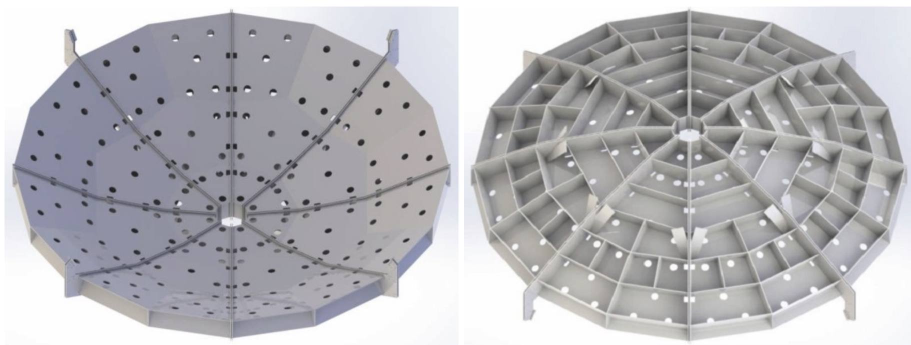

Fig. 4 The top (*left*) and rear (*right*) view of the BUS.

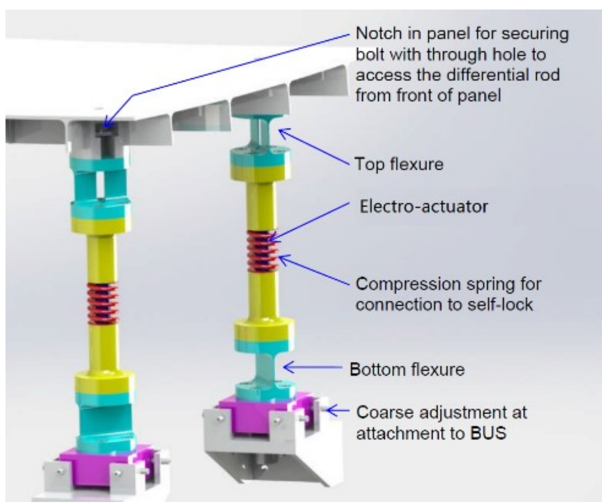

Fig. 5 Panel support structure.

Table 2 Model Mass and Material Summary

Component	Panels and Supports	BUS	Quadrapod and Apex Assembly	Transition Structure	Mount	Truss Pedestal	Entire Model
Material	Aluminum and Stainless steel	CFRP	CFRP	Steel and CFRP	Steel	Steel	/
Mass/kg Large panel layout	688	1625	69	3984	4311	3055	13732
Mass/kg Small panel layout	1247	1689	69	4099	4311	3055	14470

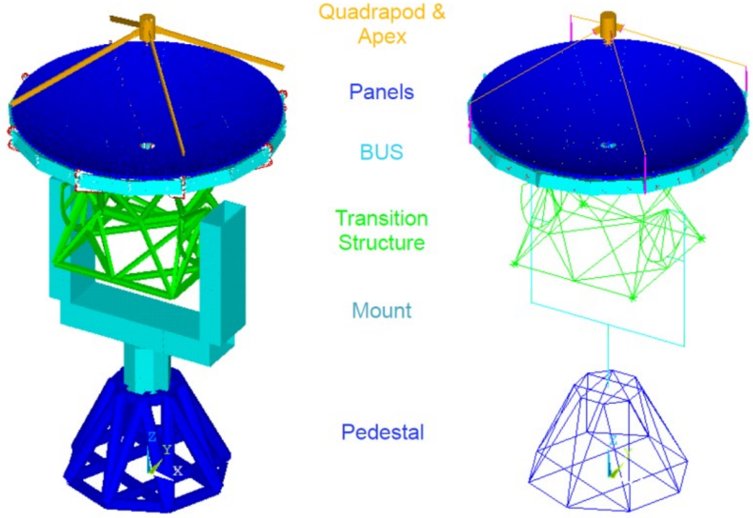

Fig. 6 Finite element model shown with extruded member cross sections (*left*) and as line elements (*right*).

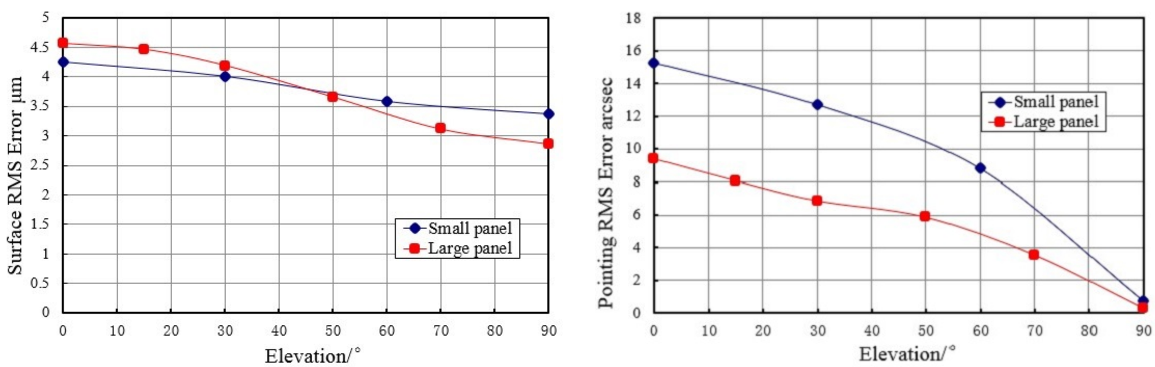

Fig. 7 Surface and pointing errors under the gravity load.

3.1 Modal Load Cases

Modal analyses are performed to compute the natural frequencies of the telescope structure, and the stiffness of the structure is investigated from the mode shapes of the structure. For this antenna, there is a direct relationship between the natural frequencies of the telescope structure and the elevation angle being set.

Table 3 shows the first five modes and their corresponding natural frequencies for the smaller panel model at elevation angles of 0°, 30°, 60° and 90°.

From Table 2, a telescope design with a higher elevation angle will have lower natural frequencies when the center of gravity of the model is higher. The structure is less rigid. From the mode shape, it can be found that there is no resonance for any substructures at low frequencies. This means that both the backup and the mounting structures meet the stiffness requirement when low frequency vibration occurs. This happens both for the larger and smaller panel designs.

3.2 Gravity Load Case

Static analysis has been performed for both gravity and temperature load cases. The FEA outputs are displacements of antenna nodes, from which surface and pointing rms errors of the main reflector for both sizes of panel layouts are derived. To calculate the surface rms error, a best fitted parabola is determined using the minimization method. The differences between the deformed nodes and the nodes on the best fitted surface are therefore derived. To compute the pointing error of the antenna, the direction of peak gain including the effect of the subreflector is calculated first. The pointing error of the main reflector is calculated by considering all the effects of displacement and tilt from the main reflector, subreflector and feed. In all calculations, the shape of the main reflector is assumed to be perfect before the loading is applied.

The surface error of the main reflector caused by gravity is mainly a function of the stiffness of the support and BUS. As seen from Figure 7, surface errors in the main

Table 3 Natural Frequencies for the First Five Modes at Four Elevation Angles

Mode	EL = 0° Freq.(Hz) Mode Shape	EL = 30° Freq.(Hz) Mode Shape	EL = 60° Freq.(Hz) Mode Shape	EL = 90° Freq.(Hz) Mode Shape
1	8.43 Side-Side Rocking	8.18 Side-Side Rocking	8.07 For-Aft Rocking	8.03 For-Aft Rocking
2	8.51 For-Aft Rocking	8.27 For-Aft Rocking	8.24 Side-Side Rocking	8.22 Side-Side Rocking
3	11.47 Mount Torsion	12.07 Mount Torsion	12.56 Mount Torsion	12.63 Mount Torsion
4	16.34 –	15.89 –	15.43 –	15.39 –
5	17.14 –	17.43 –	19.80 –	21.43 –

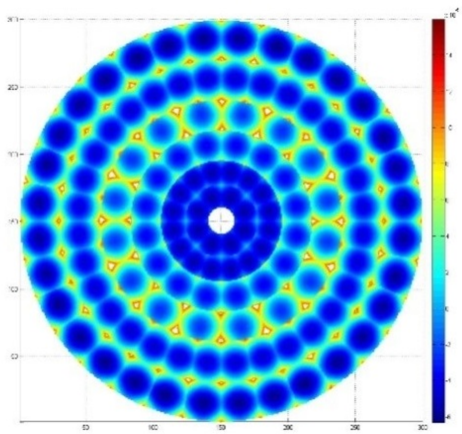

Fig. 8 Surface rms error from a thermal soak load of $-50°$C on small panel layout.

reflector caused by gravity for both layouts remain at an acceptable level of $3 \sim 4.5$ µm rms. They decline as the elevation angle increases. The pointing error for the small panel layout is larger than that for the large panel layout because the main reflector that uses the small panel structure with more adjusters is heavier. As expected, the pointing errors of both layouts are largest when pointing at the horizon and they decline to almost zero when pointing at the zenith. Since the pointing error is able to be modeled, it is easily compensated. From these analyses, the panel supports and BUS are stiff enough to maintain the shape of the surface of the main reflector under gravity.

3.3 Thermal Load Cases

Thermal load cases considered in this paper are conservative estimations from realistic weather conditions. At the Dome A site, the difference in temperature between summer and winter reaches 50°C (Bian et al. 2007; Ma et al. 2008). This is the most significant contributor to surface error for design of the aluminum panels. Simple thermal distortions of a panel can be calculated relatively easily; a uniform temperature change of dT will produce a change in curvature given by

$$dR = CTE_{\text{panel}} R dT, \tag{1}$$

where $R \approx 2f$ is the nominal radius of curvature of a paraboloid with a focal length of f and CTE_{panel} is the CTE for the panel material. The resulting rms deviation from the design surface for a square panel is

$$\sigma_{dt} = \frac{CTE_{\text{panel}} dT}{8\sqrt{3}R} d^2, \tag{2}$$

where d is the dimension of the panel. The thermal deformation trend in the panel will be strongly affected by the support structure on the panel, and it only can be obtained by the simulation results with a finite element model. So for studying the effect of the support structure on the panel when temperature changes, a loadcase of $-50°$C temperature difference is applied to the model. From results of the analysis, the best-fitted surface rms error for a small panel layout is 3.62 µm rms, while that for a large panel layout is 19.9 µm rms. From Figure 8, when the flexure-adjuster support mounted under a panel shrinks, the surface deformation of the panel is just the same as that for an isotropic structure. The thermal deformation trend of the panel without any constraint is the most optimal, and the support structures with flexure-adjuster on the panel do not undermine the trend of deformation. This verifies that the flexure-adjuster support is effective for gravity loading as it allows free-expansion of the panel in all directions.

In addition to the difference in seasonal temperature, part of thermal deformation in the main reflector comes from the vertical temperature gradient, which has been recorded at Dome A. This vertical thermal gradient can be as large as $1°\text{C m}^{-1}$, from the bottom of the main reflector to the top. To investigate the surface rms error caused by this thermal gradient alone without the effect of a change in thermal soak, the average temperature of the thermal field across the main reflector is set to be zero. Similar to the simulation with a soaking temperature $-50°$C load case, the surface error for the small panel layout is much smaller than that for the large panel layout as can be seen from Figure 9. In addition to the surface error, the pointing error also reaches a peak of $6''$ when the main reflector is pointing at the horizon. The thermal gradient across the main reflector is largest at this elevation angle.

From the above analysis, the small panel layout can meet the requirement for DATE5, especially in the thermal loading case. The last load case used includes both gravity loading and the worst possible thermal loading during Dome A's summer and winter. These loadings are applied to the small panel layout model. The vertical air temperature at Dome A has an inversion feature on the ground surface, especially in winter; the vertical temperature gradient will reach a maximum height of 4 m from the ground (Ma et al. 2010; Chen et al. 2010). The statistical mean values

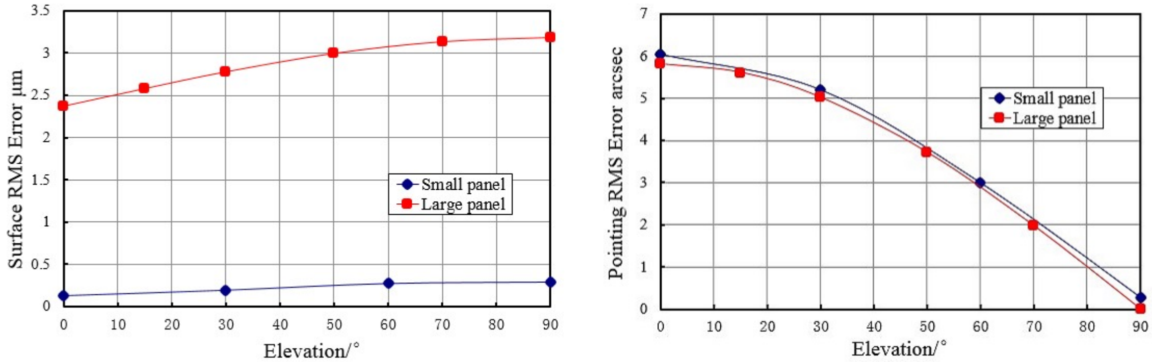

Fig. 9 Surface and pointing errors under the load of a 1°C/m vertical gradient.

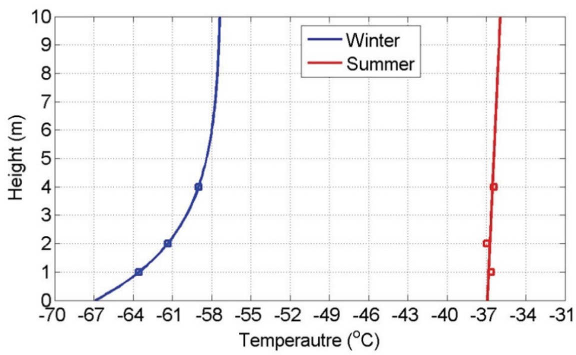

Fig. 10 The vertical air temperature distribution (0–10 m).

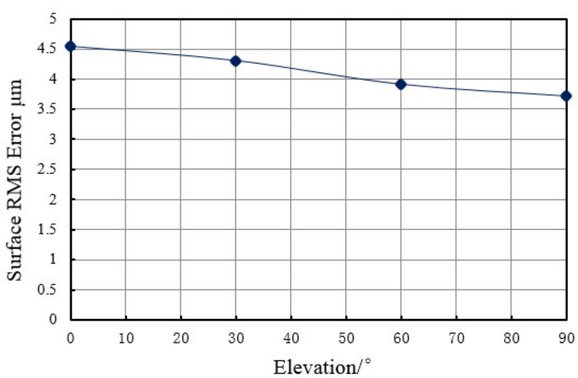

Fig. 11 The resultant surface rms error of the main reflector from summer to winter.

of temperature at vertical heights of 1 m, 2 m and 4 m are used to fit the distribution curve of air temperature in summer and winter. The fitting uses the following exponential function

$$T(h) = a - be^{-ch}, \tag{3}$$

where a, b and c are parameters used in the fit. The vertical temperature curve between a height of 0 and 10 m is shown in Figure 10.

If the surface errors of the main reflector are adjusted to make it a perfect parabola using the holographic method in the austral summer, then the simulation results also show that the surface error due to all combined loadings will be less than 4.6 µm rms in the winter, as shown in Figure 11. This result includes the various effects from gravity, change in soaking temperature and vertical temperature gradient.

3.4 PROTOTYPE PANEL

As a part of the conceptual design study, an aluminum prototype panel was produced so various tests could be applied. The prototype panel is one from the 4th ring of the small panel layout design. The prototype panel was fabricated by the CETC-39 Research Institute. The targeted surface accuracy was less than 5 µm rms. The panel was machined by using a high speed milling machine (Fig. 12, top panel). During the cutting process, the cutting force and heat were precisely controlled to avoid deformation in the panel. The final rms surface error of the prototype panel is 3.2 µm rms (Fig. 12, bottom panel).

4 SUMMARY

Table 4 summarizes surface error numbers for both large and small panel layouts. If panel setting error can be kept under 5 µm rms, then a 10 µm rms can be realizable by using state-of-the-art technologies and the small panel layout design. However, with the large panel layout, the error will be too large to be useful.

Figure 13 shows antenna diameter and reflector surface error for various submillimeter antennas including the proposed DATE5 antenna.

As discussed in this paper, although the DATE5 antenna aperture is relatively small, the DATE5 antenna is located in Antarctica, where the environmental conditions are harsher and the seasonal temperature difference is larger than those at Mauna Kea or in the Atacama Desert. By comparing with other submillimeter antennas, using aluminum panels on the DATE5 antenna has its own advantages as well as difficulties.

In summary, a conceptual design of the aluminum panel antenna for DATE5 is presented. The proposed concept includes panel structural design, panel adjusters and the BUS design. The results of FEA show:

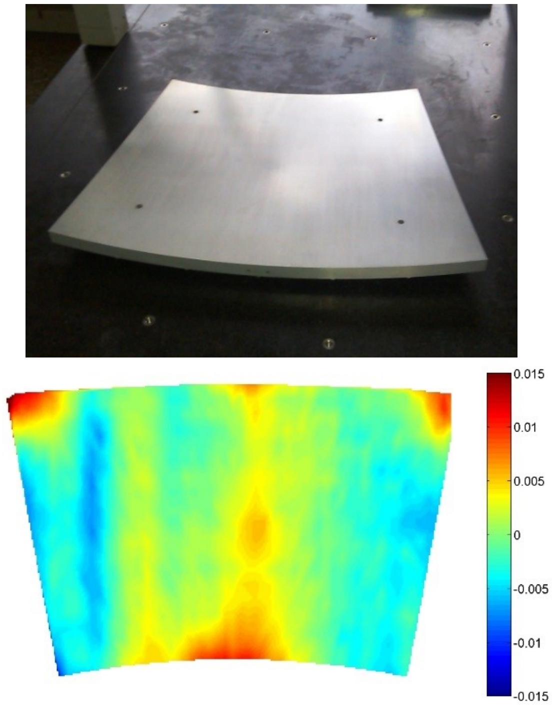

Fig. 12 Prototype panel (*top*) and measurement result of surface error (*bottom*).

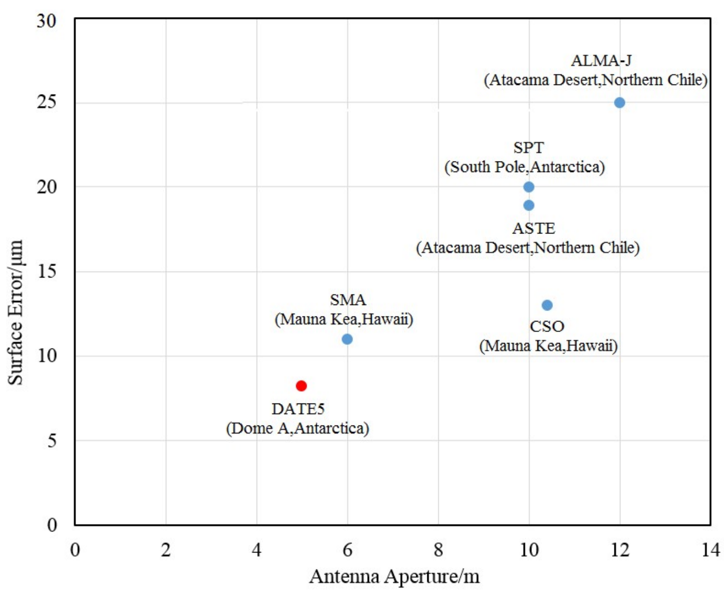

Fig. 13 A comparison between the DATE5 antenna and various submillimeter antennas.

Table 4 Model Mass and Material Summary (μm)

Component	Manufacturing	Gravity	50°C Soak	1°C/m Gradient	Setting	Total
Small panel	3.2	4.5	3.6	0.3	5	8.3
Large panel	5	4.2	19.9	3.2	5	21.7

(1) Large aluminum panels on top of a CFRP BUS concept do not meet the surface rms error budget in the soaking temperature load case. To meet this error budget, the panel size has to be reduced.
(2) Making flexures in the panel adjuster design is important to allow panels to expand freely relative to the BUS, resulting in a minimal distortion under soaking temperature load case.
(3) The improved design with small aluminum panels on the CFRP BUS is able to meet the surface rms error requirement for DATE5.

The above discussions are based on numerical simulations. The prototype aluminum panel will be tested in a climate chamber to verify its performance. Related work will be reported elsewhere.

Acknowledgements The authors have benefitted from many stimulating discussions with Steve Padin, Scott Paine, Jiasheng Huang, Qizhou Zhang and Zhong Wang. This work has been supported by the National Natural Science Foundation of China (NSFC, Grant Nos. 11190014, 11503093, 11403109 and 11373073) and the Natural Science Foundation of Jiangsu Province (Grant No. BK20141042).

References

Ali, B., Sripragash, L., & Sundaresan, M. 2011, in Proc. SPIE, 7984, Health Monitoring of Structural and Biological Systems 2011, 79841I

Bian, L., Zhang, Z., Ma, Y., Lu, L., & Chen, B. 2007, Chinese Journal of Polar Science, 2, 000

Chen, B., Zhang, R., Xiao, C., Bian, L., & Zhang, T. 2010, Chinese Science Bulletin, 55, 1430

Ezawa, H., Kawabe, R., Kohno, K., & Yamamoto, S. 2004, in Proc. SPIE, 5489, Ground-based Telescopes, ed. J. M. Oschmann, Jr., 763

Kooi, J. W., Kovács, A., Bumble, B., et al. 2004, in Proc. SPIE, 5498, Z-Spec: A Broadband Millimeter-wave Grating Spectrometer: Design, Construction, and First Cryogenic Measurements, eds. C. M. Bradford, P. A. R. Ade, J. E. Aguirre, et al. 332

Lapeyre, P., Rampini, F., Saint-Martory, G., et al. 2008, in Proc. SPIE, 7018, Advanced Optical and Mechanical Technologies in Telescopes and Instrumentation, 70181M

Leong, M., Peng, R., Houde, M., et al. 2006, in Proc. SPIE, 6275, Society of Photo-Optical Instrumentation Engineers (SPIE) Conference Series, 62750P

Ma, Y., Bian, L., Xiao, C., & Allison, I. 2008, Chinese Journal of Polar Research, 20, 299

Ma, Y., Bian, L., Xiao, C., Allison, I., & Zhou, X. 2010, Antarctic Science, 22, 443

Maldague, X. P., Shiryaev, V. V., Boisvert, É., & Vavilov, V. P. 1995, in SPIE's 1995 Symposium on OE/Aerospace Sensing and Dual Use Photonics, International Society for Optics and Photonics, 233

Raffin, P. A., Liu, C.-T., Cervera, M., et al. 2000, in Proc. SPIE, 4015, Radio Telescopes, ed. H. R. Butcher, 169

Ruhl, J., Ade, P. A. R., Carlstrom, J. E., et al. 2004, in Proc. SPIE, 5498, Z-Spec: A Broadband Millimeter-wave Grating Spectrometer: Design, Construction, and First Cryogenic Measurements, eds. C. M. Bradford, P. A. R. Ade, J. E. Aguirre, et al. 11

Ukita, N., Saito, M., Ezawa, H., et al. 2004, in Proc. SPIE, 5489, Ground-based Telescopes, ed. J. M. Oschmann, Jr., 1085

Xiao, C., Li, Y., Ian, A., et al. 2008, Annals of Glaciology, 48, 82

Yan, L., & Chen, Y. 2012, in Proc. SPIE, 8450, Modern Technologies in Space- and Ground-based Telescopes and Instrumentation II, 84505A

Yang, J., Zuo, Y.-X., Lou, Z., et al. 2013, RAA (Research in Astronomy and Astrophysics), 13, 1493